DEUTSCHES ELEKTRONEN-SYNCHROTRON DESY

DESY 71/25
May 1971

Electroproduction of $\pi^+\Delta^0(1236)$ on Hydrogen

by

C. Driver, K. Heinloth, K. Höhne,
G. Hofmann, P. Karow,
D. Schmidt, G. Specht

Deutsches Elektronen-Synchrotron DESY, Hamburg

and

J. Rathje

II. Institut für Experimentalphysik der Universität Hamburg

2 HAMBURG 52 · NOTKESTIEG 1

Electroproduction of $\pi^+\Delta^o(1236)$ on Hydrogen

by

C. Driver, K. Heinloth, K. Höhne
G. Hofmann, P. Karow,
D. Schmidt, G. Specht

Deutsches Elektronen-Synchrotron DESY, Hamburg

and

J. Rathje
II. Institut für Experimentalphysik der Universität Hamburg

Abstract

The electroproduction of a π^+-meson and of the $\Delta^o(1236)$ nucleon resonance on hydrogen, $e\ p \rightarrow e'\ \pi^+\Delta^o(1236)$, was investigated by measuring the scattered electron and the produced π^+-meson in coincidence. The differential cross sections as functions of s_o, q^2, $t-t_{min}$ or $\theta^{+}_{\pi q}$, and $\phi_{\pi q}$ were determined in the following kinematical region:

$$s_o = (\pi^+ + \Delta^o)^2 = 4.4 - 6.3\ \text{GeV}^2$$

$$|q^2| = |(e - e')^2| = 0.2 - 0.8\ \text{GeV}^2/c^2$$

$$|t - t_{min}| = 0 - 0.1\ \text{GeV}^2/c^2$$

$$\theta^*_{\pi q} = 0^o - 20^o$$

$$\phi_{\pi q} = 0 - 360^o$$

Introduction

In experiments on inelastic electron proton scattering, the total cross section for the absorption of virtual photons on protons has been measured.[1] The results show two outstanding features: This cross section as a function of the four-momentum transfer q^2 drops much less rapidly with rising $|q^2|$ than the cross section for elastic electron proton scattering. The contribution of longitudinally polarized photons to the cross section is small.

Experiments on inelastic electron scattering, detecting distinct final hadronic states, can shed more light on this behaviour.

Measurements of the electroproduction of single π^+-mesons on protons[2,3,4] show that the cross section for this reaction is dominated by a large contribution of longitudinally polarized photons in the region of small momentum transfer to the recoil nucleon. This béhaviour can be described[5] by pion exchange in the t-channel within the Electric Born Term Model and by the Vector Dominance Model. To get further information we investigated another final state, the electroproduction of a π^+-meson and of the $\Delta^0(1236)$ nucleon resonance, $e\ p \to e'\pi^+\Delta^0(1236)$ (for illustration see Fig. 1).

By detecting coincidences between the scattered electron and the produced π^+-meson the cross section has been measured as a function of the following variables;

the four-momentum squares

- of the $\pi^+\Delta^0$ system $\quad s_o = (\pi^+ + \Delta^0)^2$,
- of the virtual photon $\quad q^2 = (e - e')^2$,
- of the nucleon recoil $t-t_{min}$ $\quad t = (p - \Delta^0)^2$, t_{min} = minimum momentum transfer,

the production angle of the π^+-meson $\theta^*_{\pi q}$ in the $(\pi^+\Delta^0)$ CMS with respect to the direction of the virtual photon $\vec{q}$, and the azimuthal angle $\phi_{\pi q}$ · $\phi_{\pi q}$ is the angle between the polarization plane, subtended by $\vec{e}$ and $\vec{e}'$, and the production plane, subtended by $\vec{\pi}^+$ and $\vec{\Delta}^0$, as defined in Fig. 1.

e, e', π^+, p, Δ^0 are the four-momenta of the participating particles: The primary and the scattered electron, the π^+-meson, the target proton and the recoil nucleon resonance.

Results have been obtained in the following kinematical region:

$$4.4 \le s_o \le 6.3 \text{ GeV}^2$$
$$0.2 \le |q^2| \le 0.8 \text{ GeV}^2/c^2$$
$$0 \le |t-t_{min}| \le 0.1 \text{ GeV}^2/c^2$$
$$0^o \le \theta^*_{\pi q} \le 20^o$$
$$0 \le \phi_{\pi q} \le 360^o$$

The transverse photon polarization $\varepsilon = \left(1 + 2 \frac{\vec{q}^2}{|q^2|} \text{tg}^2 \frac{\theta_{ee'}}{2}\right)^{-1}$ varied in the range of

$$0.65 \le \varepsilon \le 0.8 \quad .$$

Assuming the validity of the one-photon exchange, the general form of the differential cross section for electroproduction of hadrons can be written as:[6]

$$\frac{d^4\sigma}{ds_o\, dq^2\, d(t-t_{min})\, d\phi_{\pi q}} = \frac{\alpha}{4(2\pi)^2} \frac{1}{E_e^2 \cdot M_p^2 \cdot |q^2|} \frac{(s_o - M_p^2)}{(1-\varepsilon)} \times$$

$$\times \left(\sigma_u(s_o, q^2, t-t_{min}) + \varepsilon\, \sigma_L(s_o, q^2, t-t_{min}) + \right.$$

$$+ \varepsilon\, \sigma_T(s_o, q^2, t-t_{min}) \cos 2\phi_{\pi q} +$$

$$\left. + \sqrt{2\varepsilon(\varepsilon+1)}\, \sigma_I(s_o, q^2, t-t_{min}) \cos\phi_{\pi q}\right) \quad . \qquad (1)$$

The cross section is separated into parts due to the two transverse and the longitudinal components of the virtual photon polarization. σ_u is the differential cross section for unpolarized transverse virtual photons. Therefoe it can be also written as the sum of the two cross sections $\sigma_{||}$ and $\sigma_{\perp}$ for transverse photons being polarized parallel and perpendicular to the production plane. In the limit $q^2 = 0$ it has to approach the cross section for unpolarized real photons. The term $\varepsilon \cdot \sigma_T \cos 2\phi_{\pi q}$ is the modification to the cross section due to the transverse linear polarization. σ_T is the difference between the two cross sections $\sigma_{||}$ $\sigma_{\perp}$. σ_L is the differential cross section for photoproduction with longitudinal polarized photons. The term $\sqrt{2\varepsilon(\varepsilon+1)}$ $\sigma_I \cos\phi_{\pi q}$ takes account for the interference between the transverse and longitudinal components $\sigma_{||}$ and σ_L of the virtual photon polarization.

By measuring the azimuthal dependence of the cross section we have separated the components $\sigma_u + \varepsilon\,\sigma_L$, σ_T and σ_I and have determined their dependence on s_o, q^2, $t-t_{min}$ and $\theta^*_{\pi q}$.

Apparatus

The apparatus is shown in Fig.2. The scattered electron and the produced π^+-meson are detected in coincidence in two spark-chamber spectrometers. After being deflected by a magnetic field both particles are detected in optical spark chambers and identified in Cherenkov and shower counters. More detail of the apparatus is given elsewhere.[2,7] The spark chamber tracks and all counter information are photographed. The pictures are analyzed automatically.[8]

Measurements

150 000 pictures have been taken for the reaction

$$ep \rightarrow e'\pi^+ \text{ (additional hadrons)}$$

at primary electron energies of 4.0, 4.9 and 5.4 GeV. By varying the energy, data could be taken in different q^2-regions keeping statistics constant. For checking the calibration of the apparatus, data on elastic electron proton scattering were also taken. The measured cross sections were consistent with the published values within 5%.[10]

Data Analysis

a) Identification of $\pi^+\Delta^o$-Events

The recorded events contain the following reactions:

$$ep \rightarrow e\ \pi^+\ n$$

$$ep \rightarrow e\ \pi^+\ \Delta^o$$

$$ep \rightarrow e\ \pi^+ \text{ (more hadrons)}$$

To separate the different reactions the mass M of the sum of all unobserved hadrons in the final state has been calculated for each event: $M^2 = (e+p-e'-\pi^+)^2$. A typical missing mass spectrum is shown in Fig.3. The excitation of the $\Delta^o(1236)$ nucleon resonance shows up as a bump around $M = 1236$ MeV/c^2.

b) Calculation of the Cross Sections

The calculation of the differential cross sections is done in a manner described elsewhere,[2,8,9] only adding the further variable M .

To get the cross sections $\frac{d^4\sigma}{ds_o\ dq^2\ d(t-t_{min})\ d\phi_{\pi q}}$, $\frac{d^4\sigma}{ds_o\ dq^2\ d\theta^*_{\pi q}\ d\phi_{\pi q}}$ for a given region ΔM , we have to integrate the fivefold differential cross section with respect to M . This procedure results in the formula

$$\frac{d^4\sigma(V_i)}{dq^2\ ds_o\ d(t-t_{min})\ d\phi_{\pi q}} = \frac{M_{ex}(\Delta V)\ S_{MC}\ F(V_i)}{N_e\ N_T\ N_{MC}(\Delta V)} \int_{\Delta M} f(V_i,M)\ dM$$

with $\Delta V = \Delta q^2\ \Delta s_o\ \Delta(t-t_{min})\ \Delta\phi_{\pi q}\ \Delta M$ five dimensional region of data taken

$V_i = \{q_i^2,\ s_{oi},\ (t-t_{min})_i,\ \phi_{\pi q_i}\}$ a point in the four dimensional space

N_e = total number of primary electrons

N_T = proton density of the target

S_{MC} = constant density of produced events in a Monte-Carlo calculation

N_{ex} = number of accepted experimental events in ΔV

N_{MC} = number of accepted Monte-Carlo events in ΔV

and $F(V) \cdot f(V,M)$, a function describing the shapes of the cross section.

c) Separation of the $\pi^+\Delta^o$ Cross Section

Within the mass region of the Δ^o-bump, in addition to $\pi^+\Delta^o$-events the radiative tail of single π^+-meson production contributes as well as multipion production. The contribution of $\pi^+\Delta^o$ was separated by fitting the mass distribution weighted by the acceptance. This fit was made for bins $\Delta q^2\ \Delta s_o\ \Delta(t-t_{min})$ assuming a relativistic Breit-Wigner formula[11] for the Δ^o-resonance, a radiative tail for single π^+ production and a polynomial including a term for the s-wave threshold behaviour of the phase-space for two-pion production.

The mass fits were done for the full mass region $1.0 \leq M \leq 1.7$ GeV/c^2, covered by this experiment in order to separate the Breit-Wigner contribution of $\pi^+\Delta^o$ from the background as cleanly as possible. A typical example is shown in Fig.4. Thus the contribution of the Δ^o in the resonance region is obtained for different parameter bins, and the cross section behaviours of $\pi^+\Delta^o$ and the background are separated. For further analysis of the reaction $\pi^+\Delta^o$ data were used from a limited missing mass interval around the Δ^o-bump with $1.14 \leq M \leq 1.34$ GeV containing 9000 events. The sum of all events in this resonance region leads to a behaviour of the cross sections which combines the dependence of the reaction $\pi^+\Delta^o$ and the dependence of the background reactions on the parameters. In the kinematic region of q^2, s_o, $t-t_{min}$ of this experiment, the contribution of $\pi^+\Delta^o$ to the measured cross section as a function of the parameters for fixed primary energy in the resonance region stays constant within ±7%. To check this behaviour of the cross sections, we also investigated for the same intervals of the parameters the cross section dependences in the higher mass regions, which are mainly made up of the background reactions. For different mass intervals from $M = 1.14$ GeV/c^2 up to $M = 1.54$ GeV/c^2 the cross section dependence on the different parameters exhibits a very similar behaviour. This fact agrees well with the constant contribution of $\pi^+\Delta^o$ found in the mass fits. To show the comparison between the cross section in the mass intervals $1.14 \leq M \leq 1.34$ GeV/c^2 and $1.34 \leq M \leq 1.54$ GeV/c^2, their dependence on s_o, $t-t_{min}$ and q^2 are given in Figs.5a, b, c. For better comparison of the dependences the data from different mass intervals are normalized in absolute height to each other by eye in order to overlap each other.

The absolute value of the cross section for $\pi^+\Delta^o$ is then obtained as the cross section of the resonance region, multiplied by the percentage of the Δ^o-contribution $P_{\Delta o}$ and further multiplied by a factor F_{BW} which cancels the loss of Δ^o due to the missing-mass cuts of the resonance region

$$\sigma_{\pi^+\Delta^o} = \sigma_{Res.Reg.} \cdot P_{\Delta^o} \cdot F_{BW}$$

with

$$F_{BW} = \int_{1.07}^{1.8} BW\, dM \Big/ \int_{1.14}^{1.34} BW\, dM$$

and BW(M) = shape of the Δ^o-resonance

$$BW(M) = M_o \cdot \frac{\Gamma(M)}{(M_o^2 - M^2)^2 + M_o^2\Gamma^2(M)}$$

$$\Gamma(M) = \Gamma(M_o) \left(\frac{q}{q_o}\right)^3 \left(\frac{a\mu^2 + q_o^2}{a\mu^2 + q^2}\right) \left(\frac{M_o}{M}\right)$$

$M_o = 1.236\ GeV/c^2$, $\Gamma(M_o) = 0.12\ GeV/c^2$, $a = 2.2\ c^2$, μ = pion mass

q , q_o = momentum of π^+ in CMS for M, M_o .

The lower limit of the integral $M = 1.07\ GeV/c^2$ is given by the pion threshold, the upper limit by the fact that the phase of Δ^o is passing 180^o at $M = 1.8\ GeV/c^2$.

Corrections

The cross section data are corrected for efficiency loss in the trigger, Cherenkov and Shower counters, for pion-interaction and pion-decay. All these corrections sum up to a value of 10% ±3%. From the total number of pictures taken, 65% were successfully analyzed by the automatic data analysis procedure and could be used for further data analysis. Rejection was mainly caused by missing sparks. It has been checked that no bias was caused by this rejection of a part of the events.

Two kinds of radiative corrections have to be considered, the radiative tail from single π^+ production and the loss by radiation. The contribution of the radiative tail is taken into account in the missing mass fitting procedure according to a behaviour $(m - m_n)^{-1}$. The second kind of radiative corrections was calculated using the method of de Calan and Fuchs.[12] These corrections do not influence the measured $\phi_{\pi q}$-dependence of the cross sections. Therefore, $\sigma_u + \varepsilon\,\sigma_L$, σ_T and σ_I can be corrected by the same percentage. In this experiment this part of the radiative corrections vary between 7% and 11% of the measured cross sections in different bins. The uncertainty of all these corrections including the uncertainty of the intensity of the primary beam add up to an systematic error less than 5%.

The main error is caused by the uncertainty of the determination of the Δ^o contribution in the missing mass fit due to the unknown missing mass shape of the background. We estimate this error to be about 20%.

Results

The measured cross sections for fixed values of q^2, s_o, $t-t_{min}$ and M are different up to a factor of 1.5 for different primary electron energies. For electron energies of 4.0, 4.9 and 5.4 GeV the contributions of the Δ^o-resonance to the cross section in the resonance region $1.14 \leq M \leq 1.34$ GeV/c^2 amounts to 42%, 33% and 27%, with an error of about ±7%. This different percentage leads to a continuous dependence of the cross section of $\pi^+\Delta^o$ with respect to the parameters q^2 and s_o.

The above mentioned differences in the measured cross sections are, therefore, caused by the background and may be partially due to the fact that the measurement at different energies implies different photon polarizations ε.
The cross sections for $\pi^+\Delta^o$ according to (1), $(\sigma_u+\varepsilon\,\sigma_L)$, σ_I and σ_T, are given as functions of s_o, q^2, $t-t_{min}$, $\theta^*_{\pi q}$, respectively. We have chosen $t-t_{min}$ as a variable instead of t because t depends strongly on q^2 and M. Taking a definite bin Δt causes restrictions to the recoil mass M. Both restrictions don't occur when choosing $t-t_{min}$, or, alternatively, $\theta^*_{\pi q}$. The dependences of the overall cross sections on s_o, q^2 and $t-t_{min}$ in the mass intervalls $1.14 \leq M \leq 1.34$ GeV/c^2 and $1.34 \leq M \leq 1.54$ GeV/c^2 are shown in Fig.5a,b,c. Their behaviour is already discussed in a previous chapter.

s_o-Dependence of $\pi^+\Delta^o$

The s_o-dependence is given in Table 1 and Fig.6 for a fixed $t-t_{min}$-value and three different q^2. The cross section is dominated by $(\sigma_u + \varepsilon\,\sigma_L)$. It shows a s_o-dependence slightly steeper than σ_u in photoproduction[13] as indicated in Fig.6. σ_I is small compared to $(\sigma_u + \varepsilon\,\sigma_L)$, and σ_T is compatible with zero. Keeping the comparison of the cross sections (Figs. 5a, b, c) in different missing mass regions in mind, the behaviour of σ_I and σ_T could be strongly influenced by the background.

$t-t_{min}$-Dependence of $\pi^+\Delta^o$

The $t-t_{min}$-dependence (Table 2 and Fig.7) is presented for a fixed s_o-value and two different q^2-values. Again $(\sigma_u + \varepsilon\,\sigma_L)$ is dominating and showing a flat decrease with $|(t-t_{min})|$. For comparison the cross section for photoproduction of $\pi^+\Delta^o$ [14] $(q^2 = 0)$ is also displayed. These values were scaled from $W = \sqrt{s_o} = 5.56$ to $W = 2.35$ GeV with an energy-dependence like $(W^2 - m_p)^{-2}$.

$\theta^*_{\pi q}$-Dependence of $\pi^+\Delta^o$

The $\theta^*_{\pi q}$- dependence (Table 3) exhibits a rather small decrease with increasing angle in the region covered by this experiment.

q^2-Dependence of $\pi^+\Delta^o$

In Table 4 and Fig.8 the q^2-dependence is shown for $s_o = 5.5\ \mathrm{GeV}^2$ and $t-t_{min} = -0.05\ \mathrm{GeV}^2/c^2$. The cross sections for $q^2 = -0.25$ and $-0.35\ \mathrm{GeV}^2/c^2$ are measured at $\sqrt{s_o} = 2.2$ GeV and have been scaled to $\sqrt{s_o} = 2.35$ GeV according to the s_o-dependence found in this experiment. For illustration a cross section behaviour according to the Vector Dominance Model $1/(m_\rho^2 - q^2)^2$ and to the Dipole fit $1/(0.71 - q^2)^4$ is shown as dotted and dashed curves, respectively.

$(\sigma_u + \varepsilon\,\sigma_L)$ decreases monotonically with increasing $|q^2|$. For comparison the photoproduction cross section at $q^2 = 0$ is also shown. The measured values of $(\sigma_u + \varepsilon\,\sigma_L)$ match with the photoproduction cross section for $q^2 = 0$. [14]

This q^2-behaviour is very different compared to the behaviour observed in single π^+-electroproduction,[2] where a dominating contribution of σ_L leads to a cross section $(\sigma_u + \varepsilon\,\sigma_L)$ increasing from the photoproduction limit up to $|q^2| \approx 0.5\mathrm{GeV}^2/c^2$. We therefore conclude that in $\pi^+\Delta^o$-production the contribution of σ_L is much smaller than in the reaction $\pi^+ n$.

Assuming a q^2-dependence of σ_u as predicted in the Vector Dominance Model[15] like $\sigma_u \sim 1/(q^2 - m_\rho^2)^2$, the ratio σ_L/σ_u has a maximum of about 0.8 around $q^2 = -0.4\ \mathrm{GeV}^2/c^2$ and drops to zero at $q^2 = 0.8\ \mathrm{GeV}^2/c^2$.

Numerical calculations for electroproduction of $\pi^+\Delta^o$ are not yet available. Therefore the results can be discussed only qualitatively.

As already mentioned above, the measured values of the transverse term σ_T are compatible with zero. σ_T is the difference between the two transverse components of the cross section for π^+-production in a plane parallel and perpendicular to the polarization plane: $\sigma_T = \frac{1}{2}(\sigma_{||} - \sigma_{\perp})$. This implies that $\sigma_{||}$ is equal to

$\sigma_\perp$. This isotropy is compatible with the measured results in photoproduction of $\pi^+\Delta^o$.[16] In the gauge invariant expanded Born-term Model[17] this means that in this region of fairly small energies the contact term dominates the one-pion exchange term (OPE).

In this frame for single π^+-electroproduction it is the OPE which gives rise to the large longitudinal contribution σ_L . Keeping this in mind, the absence of a dominating σ_L contribution in electroproduction of $\pi^+\Delta^o$ might be explained by the minor contribution of OPE to the cross section.

Acknowledgements

We wish to thank all other members of our group for their continuous whole-hearted support. We also thank Drs. A. Bartl, D. Schildknecht, W. Schmidt and D. Lüke for discussions.

Literature

1) F. Gilman, Proceedings of the Electron Photon Symposium, Liverpool (1969)

2) C. Driver, K. Heinloth, K. Höhne, G. Hofmann, P. Karow, D. Schmidt, G. Specht, J. Rathje, DESY 71/9 (1971), Phys. Lett. 35B, 77 (1971)
and Phys. Lett. 35B, 81 (1971)

3) C.N. Brown, C.R. Canizares, W.E. Cooper, A.M. Eisner, G.J. Feldman, C.A. Lichtenstein, L. Litt, W. Lockeretz, V.B. Montana, F.M. Pipkin, Phys. Rev. Lett. 26, 987 (1971)

4) P.S. Kummer, A.B. Clegg, F. Foster, G. Hughes, R. Siddle, J. Allison, B. Dickinson, E. Evangelides, M. Ibottson, R. Lawson, R.S. Meaburn, H.E. Montgomery, W.J. Shuttleworth, A. Sofair, Daresbury preprint DNPL/P 67

5) W. Schmidt, DESY 71/22 (1971);
C.N. Brown, C.R. Canizares, W.E. Cooper, A.M. Eisner, G.J. Feldman, C.A. Lichtenstein, L. Litt, W. Lockeretz, V.B. Montana, F.M. Pipkin, Phys. Rev. Lett. 26, 991 (1971);
R.C.E. Devenish, D.H. Lyth, NINA preprint (April 1971);
H. Fraas, D. Schildknecht, Phys. Lett. 35B, 75 (1971);
F.A. Berends, R. Gastmans, Harvard preprint (1971)

6) See e.g. S.M. Berman, Phys. Rev. 135, 1249 (1964)

7) J. Rathje, thesis Hamburg University (1971)

8) G. Hofmann, thesis Hamburg University (1971)

9) P. Karow, thesis Hamburg University (1971)

10) G. Weber, Proceedings of the Electron Photon Symposium, Stanford (1967)

11) A.M. Bojarski, R. Diebold, S.D. Ecklund, G.E. Fischer, Y. Murata, B. Richter, W.S.C. Williams, Phys. Rev. Lett. 22, 148 (1969)

12) C. de Calan, G. Fuchs, Nuovo Cim. 38, 1594 (1965) and Nuovo Cim. 41, 286 (1966)

13) K. Lübelsmeyer, 15th Int. Conf. on High Energy Physics, Kiev (1970)

14) A.M. Boyarski, R. Diebold, S.D. Ecklund, G.E. Fischer, Y. Murata, B. Richter, M. Sands, Phys. Rev. Lett. 25, 695 (1970)

15) J.J. Sakurai, Proceedings of the Electron Photon Symposium, Liverpool (1969)

16) C.C. Morehouse, M. Borghini, O. Chamberlain, R. Fuzesy, W. Gorn, T. Powell, P. Robrish, S. Rock, S. Shannon, G. Shapiro, H. Weisberg, A. Boyarski, S. Ecklund, Y. Murata, B. Richter, R. Siemann, R. Diebold, Phys. Rev. Lett. 25, 835 (1970)

17) P. Stichel, M. Scholz, Nuovo Cim. 34, 1381 (1964)

Table Captions

1) s_o-dependence of cross sections for fixed q^2 and $t-t_{min}$:

$$\left(\sigma_u(s_o) + \varepsilon\, \sigma_L(s_o),\ \ \sigma_I(s_o),\ \ \sigma_T(s_o)\right)_{\substack{q^2=\text{const.}\\ t-t_{min}=\text{const.}}}$$

Values of the parameters:

	data interval
$t-t_{min} = -0.05\ GeV^2/c^2$,	$-0.10 \le t-t_{min} \le 0\ GeV^2/c^2$
and $q^2 = -0.3\ GeV^2/c^2$,	$-0.40 \le q^2 \le -0.20\ GeV^2/c^2$
resp. $q^2 = -0.5\ GeV^2/c^2$,	$-0.65 \le q^2 \le -0.35\ GeV^2/c^2$
resp. $q^2 = -0.67\ GeV^2/c^2$,	$-0.80 \le q^2 \le -0.55\ GeV^2/c^2$

2) $t-t_{min}$-dependence of cross sections for fixed q^2 and s_o:

$$\left(\sigma_u(t-t_{min}) + \varepsilon\, \sigma_L(t-t_{min}),\ \ \sigma_I(t-t_{min}),\ \ \sigma_T(t-t_{min})\right)_{\substack{q^2=\text{const.}\\ s_o=\text{const.}}}$$

Values of the parameters:

	data interval
$s_o = 4.85\ GeV^2$,	$4.4 \le s_o \le 5.3\ GeV^2$
and $q^2 = -0.3\ GeV^2/c^2$,	$-0.40 \le q^2 \le -0.20\ GeV^2/c^2$
$s_o = 5.52\ GeV^2$,	$4.85 \le s_o \le 6.25\ GeV^2$
and $q^2 = -0.5\ GeV^2/c^2$,	$-0.65 \le q^2 \le -0.35\ GeV^2/c^2$
$s_o = 5.52\ GeV^2$,	$4.85 \le s_o \le 6.25\ GeV^2$
and $q^2 = -0.67\ GeV^2/c^2$,	$-0.80 \le q^2 \le -0.55\ GeV^2/c^2$

3) $\theta^{*}_{\pi q}$-dependence of cross sections for fixed q^2 and s_o:

$$\left(\sigma_u(\theta^{+}_{\pi q}) + \varepsilon\, \sigma_L(\theta^{+}_{\pi q}),\ \ \sigma_I(\theta^{+}_{\pi q}),\ \ \sigma_T(\theta^{+}_{\pi q})\right)_{\substack{q^2=\text{const.}\\ s_o=\text{const.}}}$$

Values of the parameters:

	data interval
$s_o = 4.85\ \text{GeV}^2$,	$4.4 \leq s_o \leq 5.3\ \text{GeV}^2$
and $q^2 = -0.3\ \text{GeV}^2/c^2$,	$-0.40 \leq q^2 \leq -0.20\ \text{GeV}^2/c^2$
$s_o = 5.52\ \text{GeV}^2$,	$4.85 \leq s_o \leq 6.25\ \text{GeV}^2$
and $q^2 = -0.5\ \text{GeV}^2/c^2$,	$-0.65 \leq q^2 \leq -0.35\ \text{GeV}^2/c^2$
$s_o = 5.52\ \text{GeV}^2$,	$4.85 \leq s_o \leq 6.25\ \text{GeV}^2$
and $q^2 = -0.67\ \text{GeV}^2/c^2$,	$-0.80 \leq q^2 \leq -0.55\ \text{GeV}^2/c^2$

4) q^2-dependence of cross sections for fixed s_o and $t\text{-}t_{min}$:

$$\left(\sigma_u(q^2) + \varepsilon\, \sigma_L(q^2),\ \ \sigma_I(q^2),\ \ \sigma_T(q^2)\right)_{\substack{s_o=\text{const.}\\ t-t_{min}=\text{const.}}}$$

Values of the parameters:

	data interval
$t\text{-}t_{min} = -0.05\ \text{GeV}^2/c^2$,	$-0.10 \leq t\text{-}t_{min} \leq 0\ \text{GeV}^2/c^2$
and $s_o = 4.85\ \text{GeV}^2$,	$4.4 \leq s_o \leq 5.3\ \text{GeV}^2$
resp. $s_o = 5.52\ \text{GeV}^2$	$4.85 \leq s_o \leq 6.25\ \text{GeV}^2$

Figure Captions

1) Diagram of the reaction $ep \to e\pi^+\Delta^o$

2) Experimental layout

3) Spectrum of the mass $M = \sqrt{(e+p-e'-\pi^+)^2}$ for the reaction $e + p \to e + \pi^+ +$ (additional hadrons) obtained with a primary electron energy of 4.9 GeV.

4) Spectrum of the mass $M = \sqrt{(e+p-e'-\pi^+)^2}$ for the reaction $e + p \to e + \pi^+ +$ (additional hadrons) obtained with a primary electron energy of 4.9 GeV in the data interval:

$$- 0.55 \leq q^2 \leq - 0.35 \text{ GeV}^2/c^2$$

$$4.75 \leq s_o \leq 6.25 \text{ GeV}^2$$

$$- 0.10 \leq t-t_{min} \leq 0.0 \text{ GeV}^2/c^2$$

Results of the fit to this distribution for Δ^o and background are included.

5) Comparison of the cross sections in the different mass regions

$$1.14 \leq M \leq 1.34 \text{ GeV} \quad \text{and}$$

$$1.34 \leq M \leq 1.54 \text{ GeV}.$$

a) s_o-dependence

Values of the parameters:	data interval
$t-t_{min} = - 0.05$ GeV^2/c^2	$- 0.10 \leq t-t_{min} \leq 0.0$ GeV^2/c^2
and $q^2 = - 0.5$ GeV^2/c^2	$- 0.65 \leq q^2 \leq - 0.35$ GeV^2/c^2
resp. $q^2 = - 0.67$ GeV^2/c^2	$- 0.80 \leq q^2 \leq - 0.55$ GeV^2/c^2

b) $t-t_{min}$-dependence

Values of the parameters:

Values of the parameters	data interval
$s_o = 5.5\ GeV^2$	$4.85 \leq s_o \leq 6.25\ GeV^2$
and $q^2 = -0.5\ GeV^2/c^2$	$-0.65 \leq q^2 \leq -0.35\ GeV^2/c^2$
resp. $q^2 = -0.67\ GeV^2/c^2$	$-0.80 \leq q^2 \leq -0.55\ GeV^2/c^2$

c) q^2-dependence

Values of the parameters:

Values of the parameters	data interval
$t-t_{min} = -0.05\ GeV^2/c^2$	$-0.10 \leq t-t_{min} \leq 0\ GeV^2/c^2$
and $s_o = 5.5\ GeV^2$	$4.85 \leq s_o \leq 6.25\ GeV^2$

6) s_o-dependence of the cross sections

$\sigma_u + \varepsilon\,\sigma_L$, σ_I and σ_T for fixed q^2 and $t-t_{min}$

Values of the parameters:

Values of the parameters	data interval
$t-t_{min} = -0.05\ GeV^2/c^2$	$-0.10 \leq t-t_{min} \leq 0\ GeV^2/c^2$
and $q^2 = -0.3\ GeV^2/c^2$	$-0.40 \leq q^2 \leq -0.20\ GeV^2/c^2$
resp. $q^2 = -0.5\ GeV^2/c^2$	$-0.65 \leq q^2 \leq -0.35\ GeV^2/c^2$
resp. $q^2 = -0.67\ GeV^2/c^2$	$-0.80 \leq q^2 \leq -0.55\ GeV^2/c^2$

Dashed lines show comparison with the s_o-dependence in photoproduction (normalized arbitrarily).

7) $t-t_{min}$-dependence of the cross sections

$\sigma_u + \varepsilon\,\sigma_L$, σ_I and σ_T for fixed q^2 and s_o

Values of the parameters:

Values of the parameters	data interval
$s_o = 4.85\ GeV^2$	$4.4 \leq s_o \leq 5.3\ GeV^2$
and $q^2 = -0.3\ GeV^2/c^2$	$-0.40 \leq q^2 \leq -0.20\ GeV^2/c^2$
$s_o = 5.52\ GeV^2$	$4.85 \leq s_o \leq 6.25\ GeV^2$
and $q^2 = -0.5\ GeV^2/c^2$	$-0.65 \leq q^2 \leq -0.35\ GeV^2/c^2$
$s_o = 5.52\ GeV^2$	$4.85 \leq s_o \leq 6.25\ GeV^2$
and $q^2 = -0.67\ GeV^2/c^2$	$-0.80 \leq q^2 \leq -0.55\ GeV^2/c^2$

8) q^2-dependence of cross sections

$\sigma_u + \varepsilon\, \sigma_L$, σ_I, σ_T for fixed s_o and $t\text{-}t_{min}$

Values of the parameters:

Values of the parameters	data interval
$t\text{-}t_{min} = -\,0.05\ GeV^2/c^2$	$-\,0.10 \leq t\text{-}t_{min} \leq 0.0\ GeV^2/c^2$
and $s_o = 4.85\ GeV^2$	$4.4 \leq s_o \leq 5.3\ GeV^2$
resp. $s_o = 5.52\ GeV^2$	$4.85 \leq s_o \leq 6.25\ GeV^2$

For illustration a behavior according to the Vector Dominance Model $\left(\frac{m_\rho^2}{m_\rho^2 - q^2}\right)^2$ and to the Dipole Fit $\left(\frac{0.71}{q^2 - 0.71}\right)^4$ is shown as dotted and dashed curves, respectively.

Table 1 s_o-Dependence of Cross Sections $\sigma_u + \varepsilon\, \sigma_L$, σ_I and σ_T for Fixed q^2 and $t-t_{min}$

E (GeV)	ε	$-q^2$ ($\frac{GeV^2}{c^2}$)	$\lvert t-t_{min}\rvert$ ($\frac{GeV^2}{c^2}$)	$\sqrt{s_o}$ (GeV)	$\sigma_u + \varepsilon\, \sigma_L$ ($\pi^+\Delta^o$ + background) ($\frac{\mu b}{GeV^2}$)	stat. error	fraction of $\pi^+\Delta^o$ P_{Δ^o}	BW factor F_{BW}	$\sigma_u + \varepsilon\, \sigma_L$ ($\pi^+\Delta^o$) (rad. corr. included) ($\frac{\mu b}{GeV^2}$)	stat. error	rad. corr. (%)
4.0	0.78	0.3	0.05	2.13	24.2	1.6	.42	1.39	15.1	1.0	7.2
	0.72	0.3	0.05	2.19	23.5	2.5			14.7	1.6	7.1
4.9	0.80	0.5	0.05	2.20	15.8	1.3	.33	1.39	8.0	0.7	9.5
	0.78	0.5	0.05	2.25	13.6	0.9			6.8	0.4	9.3
	0.75	0.5	0.05	2.30	10.7	0.8			5.4	0.4	9.2
5.4	0.80	0.67	0.05	2.25	10.7	1.0	.27	1.39	4.4	0.4	10.7
	0.77	0.67	0.05	2.32	7.8	0.5			3.2	0.2	10.5
	0.72	0.67	0.05	2.43	4.3	0.2			1.8	0.1	10.1

Table 1 continued

E GeV	ε	$-q^2$ $\frac{GeV^2}{c^2}$	$\lvert t-t_{min}\rvert$ $\frac{GeV^2}{c^2}$	$\sqrt{s_o}$ GeV	σ_I ($\pi^+\Delta^o$ + background) $\frac{\mu b}{GeV^2}$	stat. error	fraction of $\pi^+\Delta^o$ P_{Δ^o}	BW factor F_{BW}	σ_I ($\pi^+\Delta^o$) (rad.corr.included) $\frac{\mu b}{GeV^2}$	stat. error	rad. corr. %
4.0	0.78	0.3	0.05	2.13	9.5	3.8	.42	1.39	5.9	2.3	7.2
	0.72	0.3	0.05	2.19	0.8	6.2			0.5	3.9	7.1
4.9	0.80	0.5	0.05	2.20	3.6	3.2	.33	1.39	1.8	1.7	9.5
	0.78	0.5	0.05	2.25	6.9	2.1			3.5	1.1	9.3
	0.75	0.5	0.05	2.30	5.1	2.0			2.5	1.1	9.2
5.4	0.80	0.67	0.05	2.25	2.2	2.4	.27	1.39	0.9	1.1	10.7
	0.77	0.67	0.05	2.32	3.6	1.2			1.5	0.5	10.5
	0.72	0.67	0.05	2.43	3.6	0.3			1.5	0.2	10.1
					σ_T				σ_T		
4.0	0.78	0.3	0.05	2.13	- 1.4	3.3	.42	1.39	- 0.9	2.1	7.2
	0.72	0.3	0.05	2.19	3.3	3.6			2.0	2.3	7.1
4.9	0.80	0.5	0.05	2.20	1.3	2.4	.33	1.39	0.7	1.2	9.5
	0.78	0.5	0.05	2.25	0.7	1.8			0.35	1.1	9.3
	0.75	0.5	0.05	2.30	0.7	1.7			0.35	0.8	9.2
5.4	0.80	0.67	0.05	2.25	- 0.3	1.7	.27	1.39	- 0.12	0.6	10.7
	0.77	0.67	0.05	2.32	0.4	1.1			0.17	0.5	10.5
	0.72	0.67	0.05	2.43	- 0.5	0.3			- 0.21	0.2	10.1

Table 2 $t-t_{min}$-Dependence of Cross Sections for Fixed q^2 and s_o

					cross section for $\pi^+\Delta^o$+background								cross section for $\pi^+\Delta^o$						
E (GeV)	ε	$-q^2$ ($\frac{GeV^2}{c^2}$)	$\|t-t_{min}\|$ ($\frac{GeV^2}{c^2}$)	$\sqrt{s_o}$ (GeV)	$\sigma_u+\varepsilon\sigma_L$ ($\frac{\mu b}{GeV^2}$)	stat. error	σ_I ($\frac{\mu b}{GeV^2}$)	stat. error	σ_T ($\frac{\mu b}{GeV^2}$)	stat. error	fraction of $\pi^+\Delta^o$ P_{Δ^o}	BW factor F_{BW}	$\sigma_u+\varepsilon\sigma_L$ ($\frac{\mu b}{GeV^2}$)	stat. error	σ_I ($\frac{\mu b}{GeV^2}$)	stat. error	σ_T ($\frac{\mu b}{GeV^2}$)	stat. error	rad. corr. (%)
4.0	0.72	0.3	0.009	2.2	22.7	1.5	4.2	2.3	-0.4	1.7	.42	1.39	14.3	1.0	2.7	2.3	-0.25	1.7	7.4
	0.72	0.3	0.031	2.2	27.2	3.8	-7.5	6.2	6.7	3.3			16.9	2.4	-4.7	5.9	4.3	3.0	7.2
	0.72	0.3	0.060	2.2	19.8	5.6	-1.0	8.9	3.3	4.7			12.4	3.5	-0.6	8.6	2.0	4.5	7.0
4.9	0.72	0.5	0.007	2.35	11.1	0.6	1.7	0.8	0.3	0.8	.33	1.39	5.6	0.3	0.9	0.6	0.15	0.6	9.4
	0.72	0.5	0.025	2.35	9.9	0.7	4.3	1.1	0.5	0.9			4.9	0.3	2.2	0.8	0.25	0.6	9.2
	0.72	0.5	0.047	2.35	8.3	0.9	5.1	1.5	-0.3	1.2			4.1	0.4	2.5	1.2	-0.15	1.1	9.0
	0.72	0.5	0.072	2.35	9.9	1.8	-2.6	2.9	4.0	1.8			4.9	0.9	-1.3	2.1	2.0	1.4	8.8
	0.72	0.5	0.102	2.35	9.2	3.0	0.0	4.7	1.6	2.7			4.6	1.5	0	3.6	0.78	2.0	8.6
5.4	0.76	0.67	0.007	2.35	7.9	0.4	1.0	0.6	1.9	0.6	.27	1.39	3.31	0.17	0.4	0.3	0.8	0.3	10.8
	0.76	0.67	0.027	2.35	8.4	0.4	0.9	0.6	-0.3	0.6			3.51	0.17	0.3	0.3	-0.1	0.3	10.6
	0.76	0.67	0.052	2.35	6.6	0.5	1.5	0.8	0.2	0.8			2.8	0.2	0.6	0.5	0.1	0.5	10.4
	0.76	0.67	0.077	2.35	6.1	0.9	1.7	1.4	-1.2	1.2			2.5	0.41	0.61	0.9	-0.5	0.9	10.2
	0.76	0.67	0.102	2.35	5.1	1.5	-0.3	1.9	0.5	2.1			2.1	0.6	-0.1	1.2	0.2	1.4	10.0

Table 3 $\theta^{*}_{\pi q}$-Dependence of Cross Sections for Fixed q^2 and s_o

E	ε	$-q^2$	$\theta^{*}_{\pi q}$	$\sqrt{s_o}$	cross section for $\pi^+\Delta^o$+background $\sigma_u+\varepsilon\sigma_L$	stat. error	σ_I	stat. error	σ_T	stat. error	fraction of $\pi^+\Delta^o$ P_{Δ^o}	BW factor F_{BW}	cross section for $\pi^+\Delta^o$ $\sigma_u+\varepsilon\sigma_L$	stat. error	σ_I	stat. error	σ_T	stat. error	rad. corr.
GeV		$\frac{GeV^2}{c^2}$	°	GeV	$\frac{\mu b}{GeV^2}$		$\frac{\mu b}{GeV^2}$		$\frac{\mu b}{GeV^2}$				$\frac{\mu b}{GeV^2}$		$\frac{\mu b}{GeV^2}$		$\frac{\mu b}{GeV^2}$		%
4.0	0.72	0.3	2.5	2.2	31.7	2.7	1.0	2.6	-2.1	4.9	.42	1.39	19.9	1.7	0.6	2.4	-1.6	4.6	7.6
	0.72	0.3	7.5	2.2	31.6	3.4	0.4	3.6	-0.6	4.7			19.8	2.3	0.3	3.4	-0.4	4.5	7.4
	0.72	0.3	12.0	2.2	30.1	5.0	-3.2	5.2	7.0	6.2			18.9	3.1	-2.0	4.8	4.4	5.8	7.2
	0.72	0.3	16.0	2.2	21.9	6.0	2.8	6.2	2.9	7.6			13.6	3.8	1.8	5.8	1.8	7.2	7.0
4.9	0.72	0.5	2.5	2.35	19.5	1.5	-0.4	1.8	6.6	3.8	.33	1.39	9.8	0.8	-0.2	1.4	3.3	2.8	9.5
	0.72	0.5	7.5	2.35	16.3	0.9	5.4	1.0	-2.8	2.3			8.2	0.5	2.7	0.8	-1.4	1.7	9.3
	0.72	0.5	12.0	2.35	16.7	1.7	2.3	2.2	2.0	3.6			8.4	0.9	1.2	1.6	1.0	2.7	9.0
	0.72	0.5	16.0	2.35	12.6	2.0	2.0	2.4	1.3	4.1			6.3	1.0	1.0	1.8	3.6	3.0	8.8
	0.72	0.5	21.5	2.35	16.4	4.9	-3.6	5.7	4.9	8.7			8.1	2.4	-1.8	4.2	2.4	6.4	8.5
5.4	0.76	0.67	2.5	2.35	14.2	1.1	2.5	1.3	-0.6	3.2	.27	1.39	5.9	0.5	1.0	0.7	-0.2	1.9	11.0
	0.76	0.67	7.5	2.35	15.4	0.8	0.9	1.0	1.0	2.2			6.3	0.3	0.4	0.6	0.4	1.4	10.7
	0.76	0.67	12.0	2.35	13.5	1.0	3.1	1.2	-0.6	2.6			5.6	0.4	1.3	0.8	-0.2	1.6	10.2
	0.76	0.67	16.0	2.35	11.1	1.6	4.3	1.8	-3.1	4.4			4.6	0.7	1.8	1.1	-1.3	2.7	10.0

Table 4 q^2-Dependence of Cross Sections for Fixed s_o and $t-t_{min}$

					cross section for $\pi^+\Delta^o$+background								cross section for $\pi^+\Delta^o$						
E	ε	$-q^2$	$\|t-t_{min}\|$	$\sqrt{s_o}$	$\sigma_u+\varepsilon\sigma_L$	stat. error	σ_I	stat. error	σ_T	stat. error	fraction of $\pi^+\Delta^o$	BW factor	$\sigma_u+\varepsilon\sigma_L$	stat. error	σ_I	stat. error	σ_T	stat. error	rad. corr.
GeV		$\frac{GeV^2}{c^2}$	$\frac{GeV^2}{c^2}$	GeV	$\frac{\mu b}{GeV^2}$		$\frac{\mu b}{GeV^2}$		$\frac{\mu b}{GeV^2}$		P_{Δ^o}	F_{BW}	$\frac{\mu b}{GeV^2}$		$\frac{\mu b}{GeV^2}$		$\frac{\mu b}{GeV^2}$		%
4.0	0.73	0.25	0.05	2.2	20.1	2.0	7.8	3.2	0.7	1.9	.42	1.39	12.6	1.3	4.9	3.0	0.4	1.8	6.8
	0.70	0.35	0.05	2.2	19.1	1.2	5.6	1.9	-0.2	1.6			12.0	0.8	3.5	1.8	-0.13	1.5	7.2
4.9	0.77	0.4	0.05	2.35	12.1	1.1	4.4	1.8	1.4	1.2	.33	1.39	6.1	0.5	2.2	1.4	0.7	1.1	8.6
	0.75	0.5	0.05	2.35	9.5	0.4	4.0	0.7	0.4	0.6			4.8	0.2	2.0	0.5	0.2	0.5	9.0
	0.74	0.6	0.05	2.35	6.1	0.5	1.3	0.8	-0.2	0.7			3.1	0.2	0.7	0.6	0.1	0.5	9.3
5.4	0.77	0.6	0.05	2.35	9.1	0.5	3.2	0.8	1.2	0.7	.27	1.39	3.8	0.2	1.3	0.5	0.5	0.5	10.2
	0.76	0.7	0.05	2.35	6.7	0.3	1.6	0.5	-0.5	0.5			2.8	0.1	0.7	0.3	-0.2	0.3	10.5
	0.74	0.8	0.05	2.35	4.2	0.5	0.9	0.8	0.0	0.6			1.8	0.2	0.4	0.5	0.0	0.3	10.7

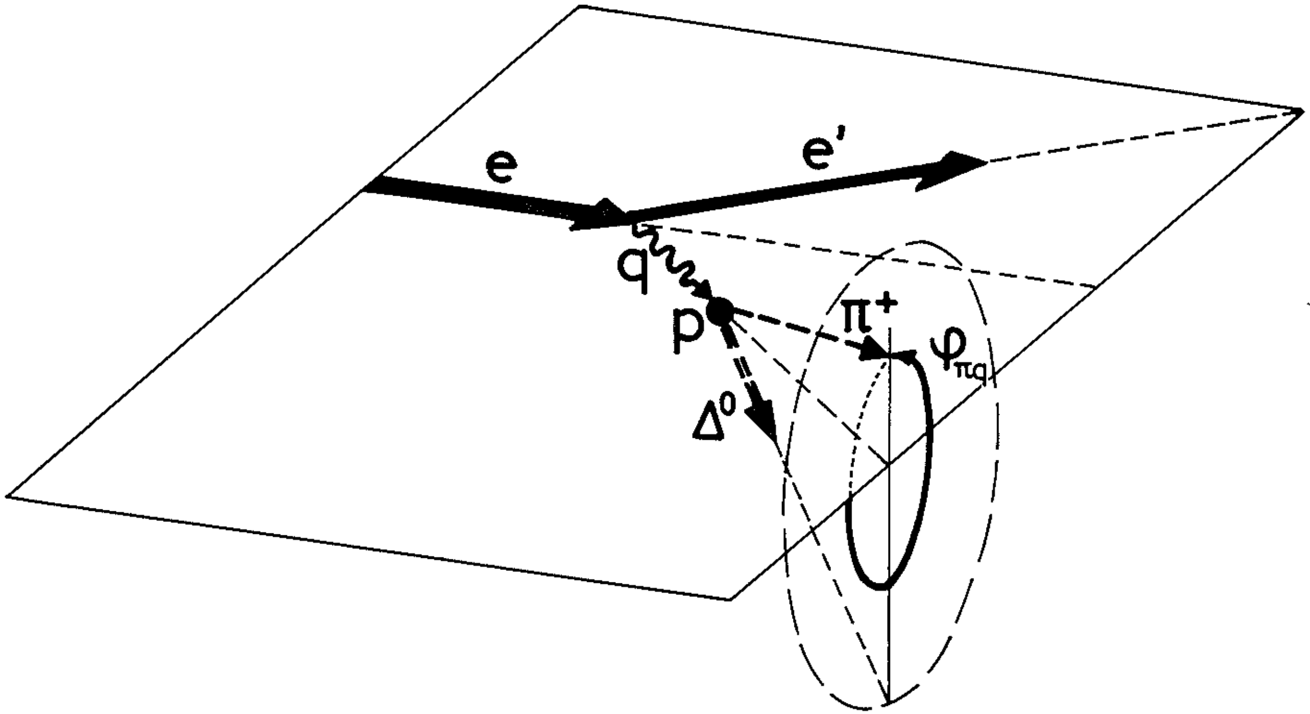

Fig. 1

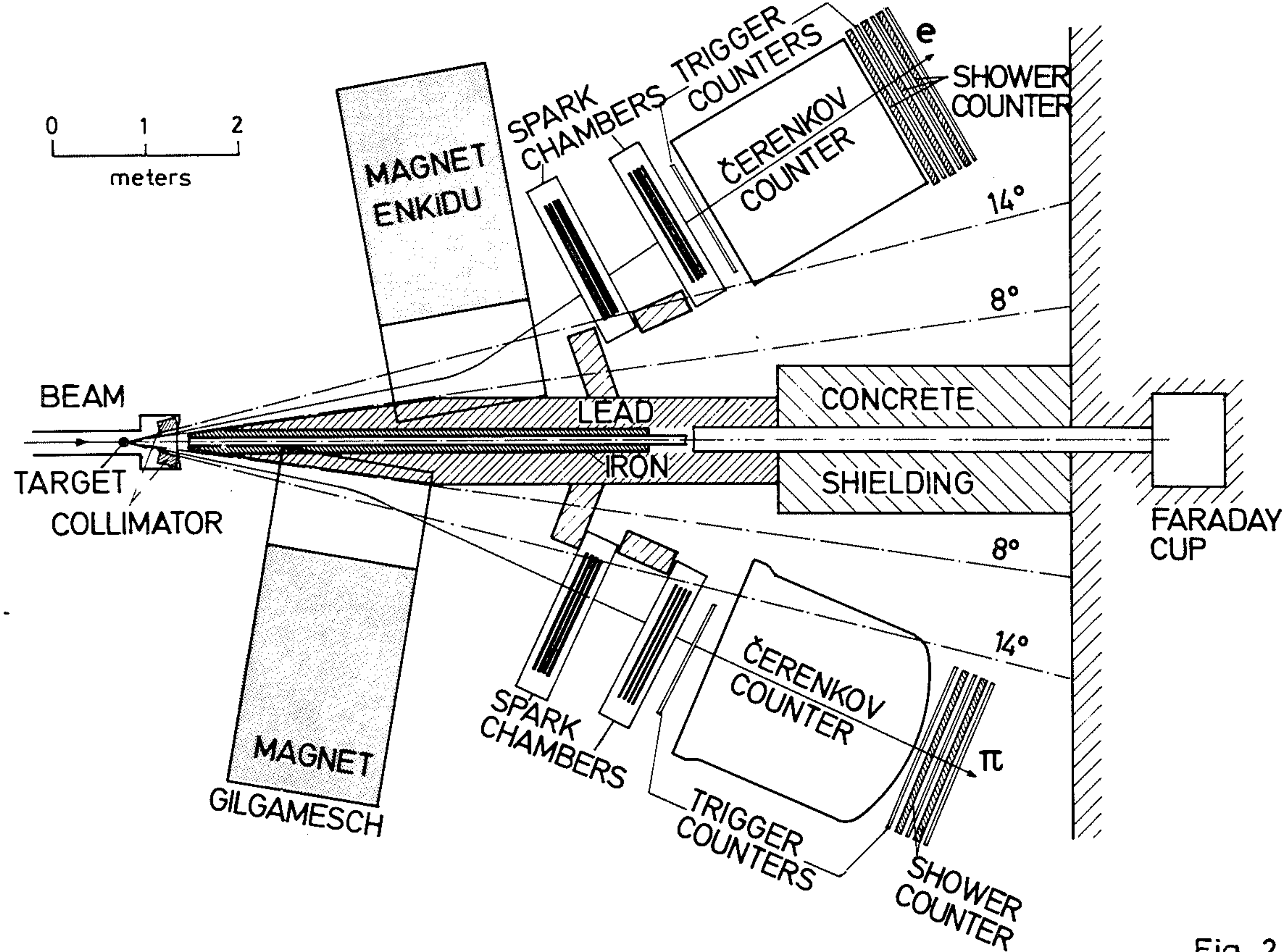
0
1
2
meters
MAGNET
ENKIDU
SPARK
CHAMBERS
TRIGGER
COUNTERS
ČERENKOV
COUNTER
e
SHOWER
COUNTER
14°
8°
BEAM
TARGET
COLLIMATOR
LEAD
IRON
CONCRETE
SHIELDING
FARADAY
CUP
8°
14°
MAGNET
GILGAMESCH
SPARK
CHAMBERS
TRIGGER
COUNTERS
ČERENKOV
COUNTER
π
SHOWER
COUNTER

Fig. 2

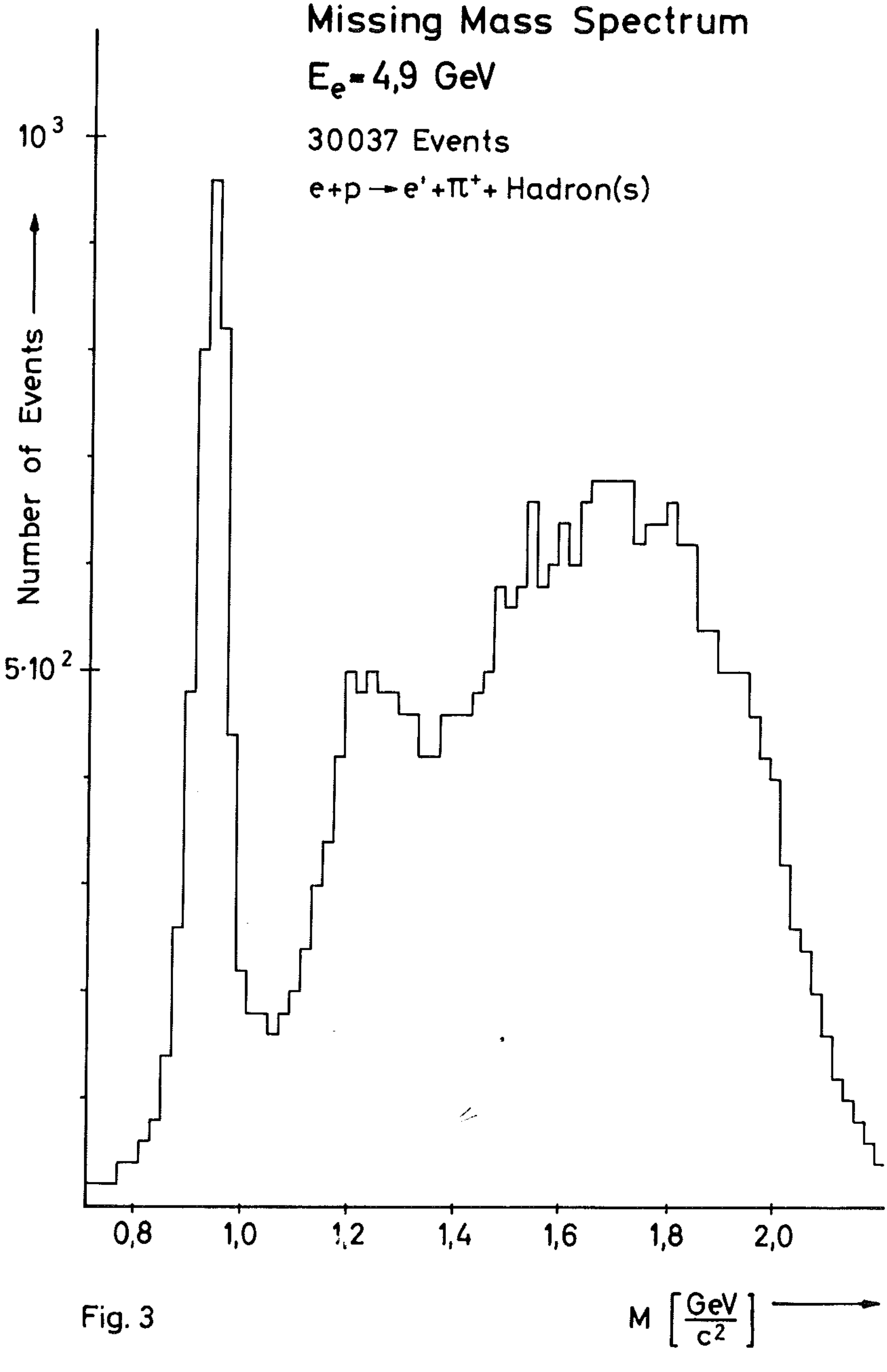

Missing Mass Spectrum
$E_e = 4,9$ GeV
30037 Events
$e+p \rightarrow e'+\pi^+ +$ Hadron(s)
10^3
$5\cdot10^2$
Number of Events
0,8
1,0
1,2
1,4
1,6
1,8
2,0
M $\left[\frac{GeV}{c^2}\right]$

Fig. 3

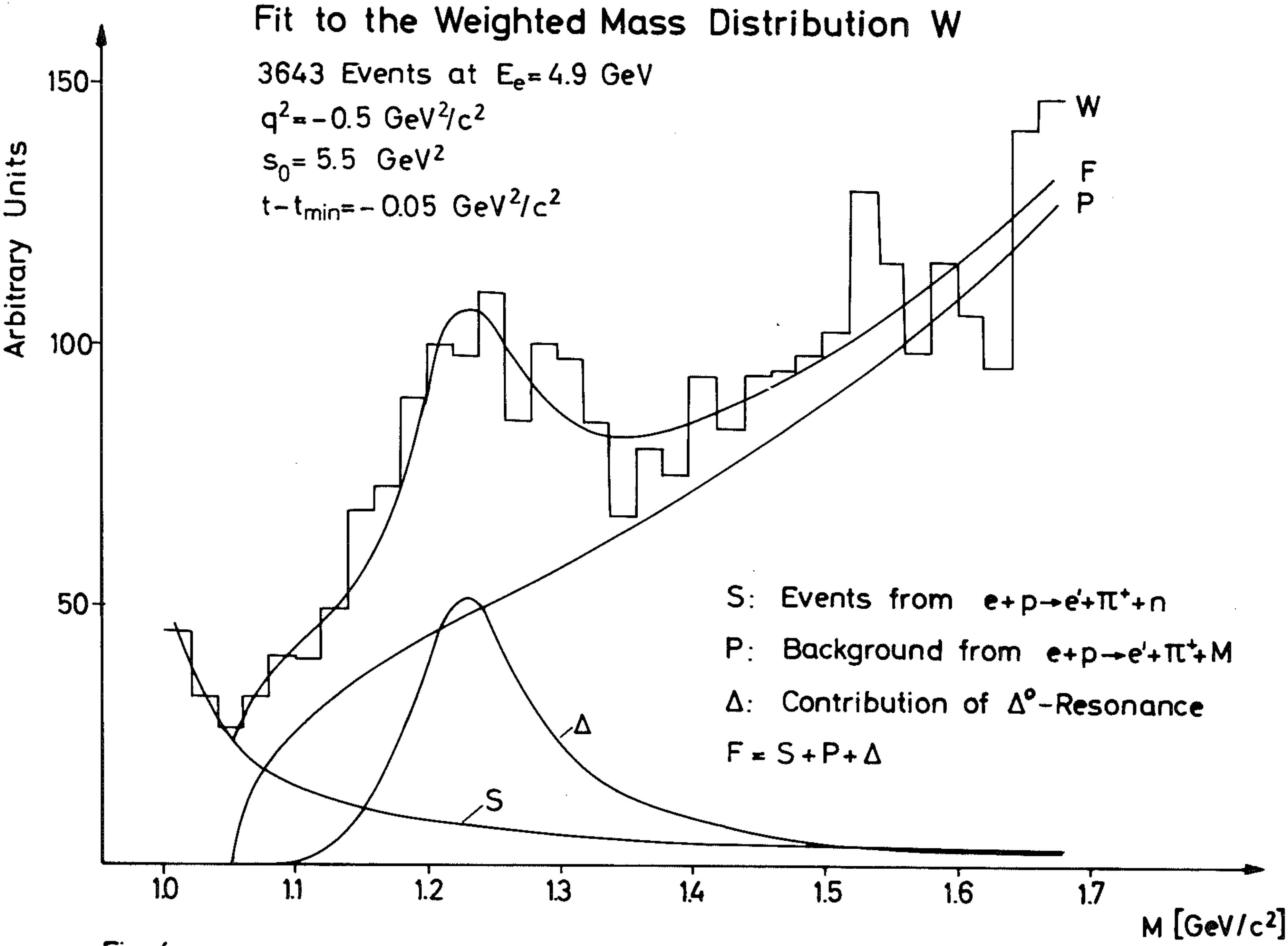
Fit to the Weighted Mass Distribution W
3643 Events at $E_e = 4.9$ GeV
$q^2 = -0.5$ GeV^2/c^2
$s_0 = 5.5$ GeV^2
$t - t_{min} = -0.05$ GeV^2/c^2
Arbitrary Units
150
100
50
W
F
P
Δ
S
S: Events from $e + p \rightarrow e' + \pi^+ + n$
P: Background from $e + p \rightarrow e' + \pi^+ + M$
Δ: Contribution of Δ^0-Resonance
F = S + P + Δ
1.0
1.1
1.2
1.3
1.4
1.5
1.6
1.7
M [GeV/c^2]

Fig. 4

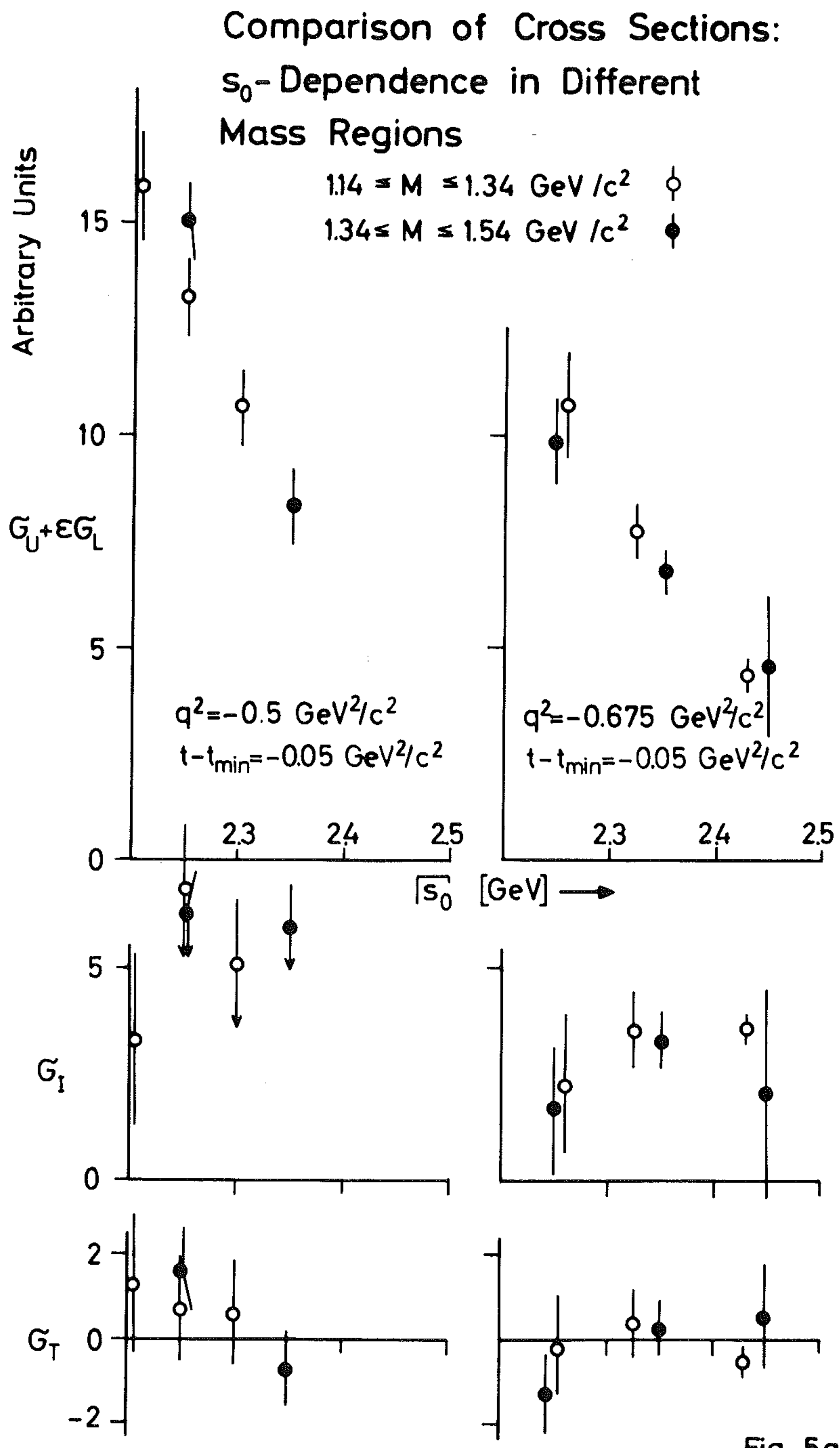
Comparison of Cross Sections:
s0-Dependence in Different
Mass Regions
1.14 ≤ M ≤ 1.34 GeV/c²
1.34 ≤ M ≤ 1.54 GeV/c²
Arbitrary Units
15
10
5
0
5
0
2
0
-2
σU+εσL
σI
σT
q²=-0.5 GeV²/c²
t-tmin=-0.05 GeV²/c²
q²=-0.675 GeV²/c²
t-tmin=-0.05 GeV²/c²
2.3
2.4
2.5
2.3
2.4
2.5
√s0 [GeV]

Fig. 5a

Comparison of Cross Sections: $(t-t_{min})$ Dependence in Different Mass Regions

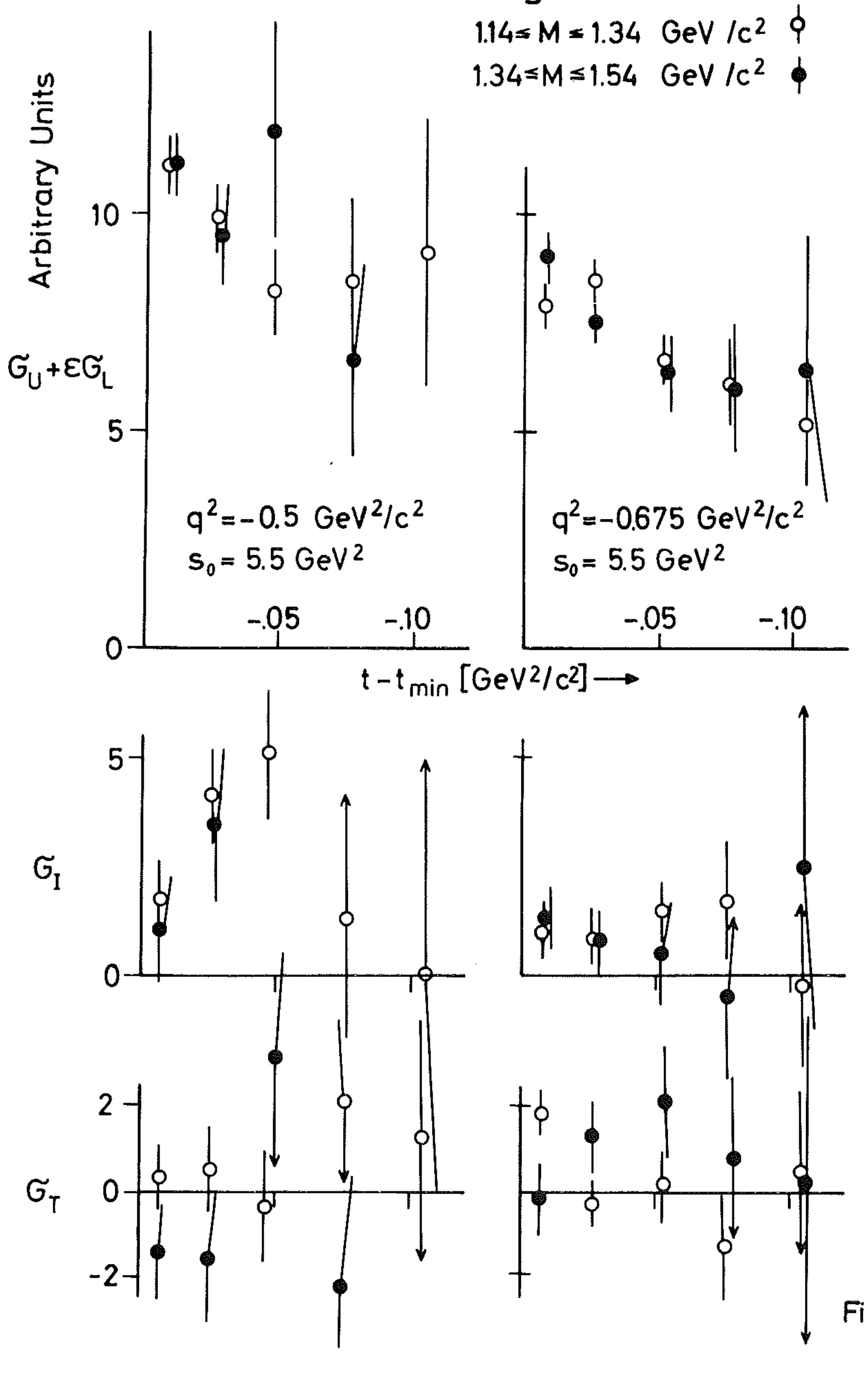

Fig. 5b

Comparison of Cross Sections: q^2-Dependence in Different Mass Regions

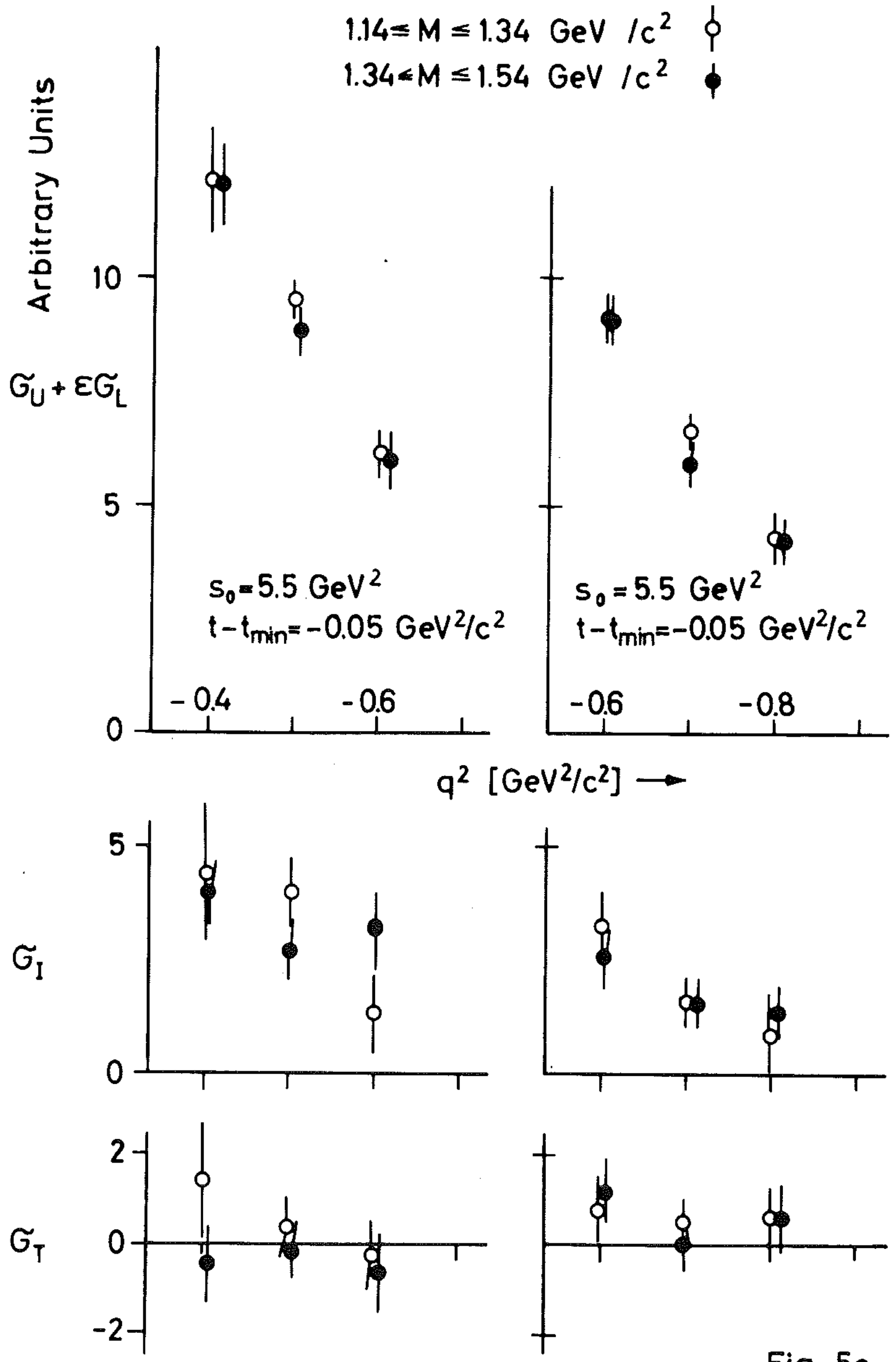

Fig. 5c

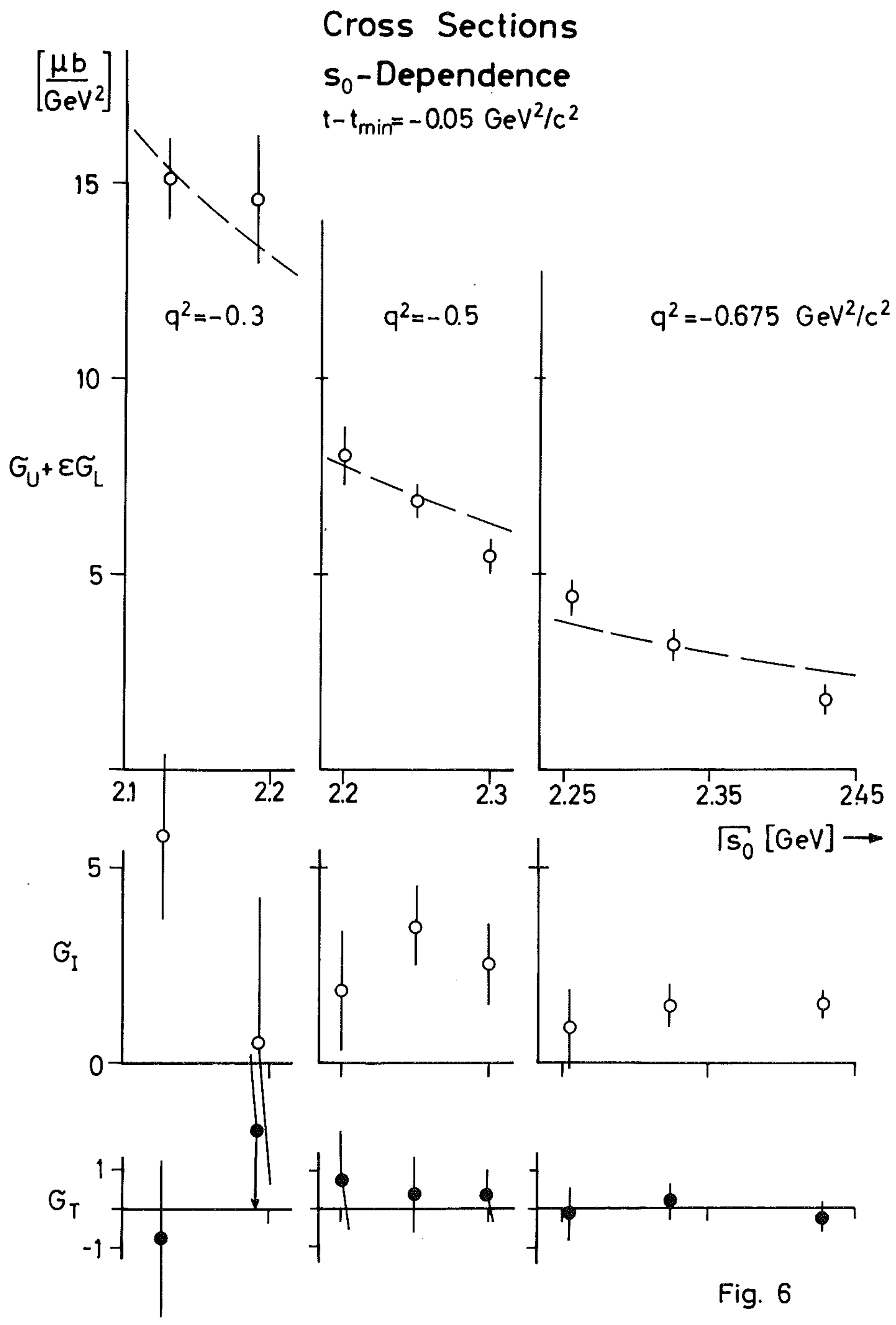
Cross Sections
s0-Dependence
t-tmin=-0.05 GeV2/c2
[μb/GeV2]
15
10
5
0
5
1
-1
q2=-0.3
q2=-0.5
q2=-0.675 GeV2/c2
GU+εGL
GI
GT
2.1
2.2
2.2
2.3
2.25
2.35
2.45
√s0 [GeV]

Fig. 6

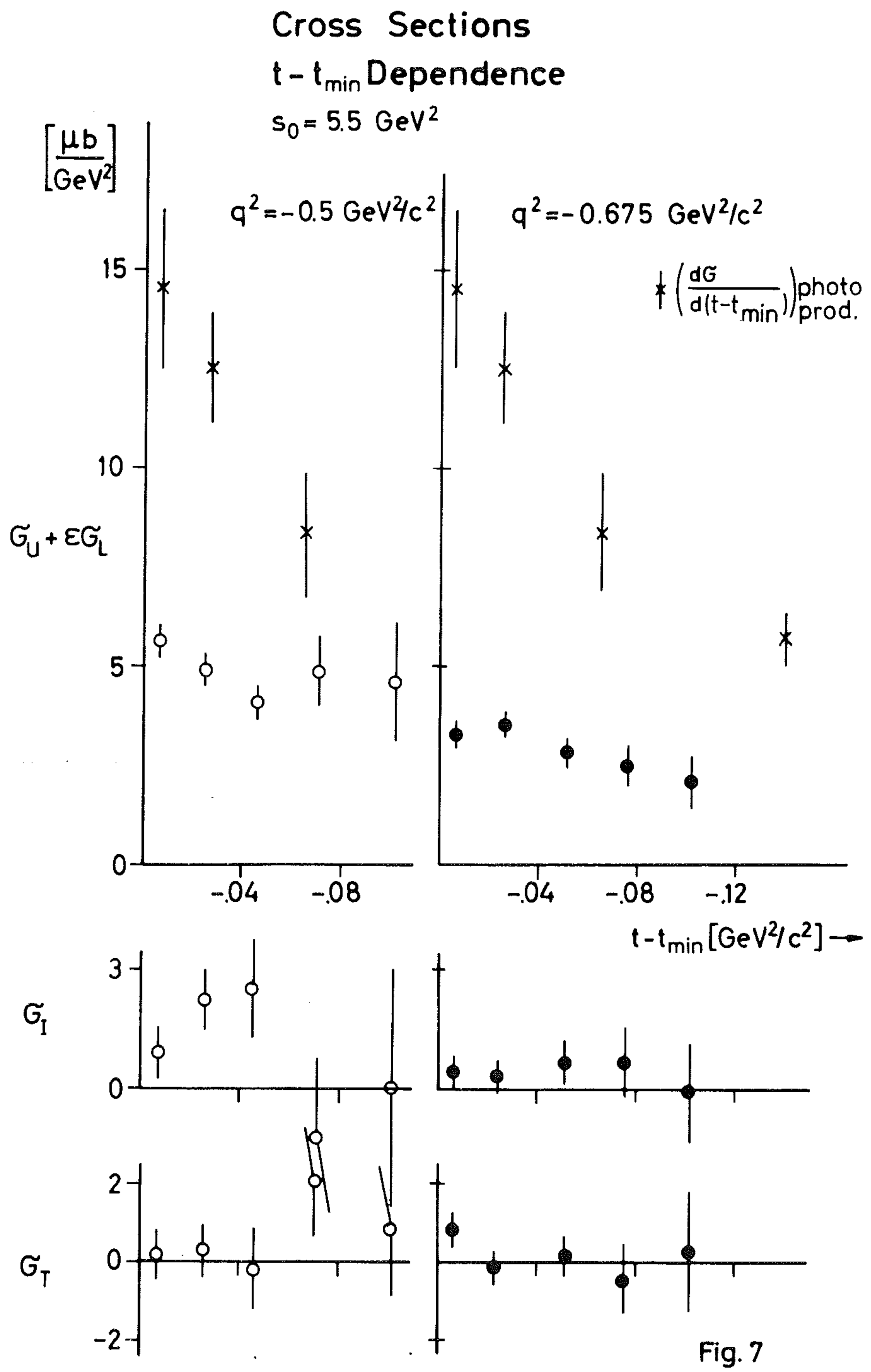

Cross Sections
t - t_min Dependence
s_0 = 5.5 GeV^2
[μb/GeV^2]
q^2 = -0.5 GeV^2/c^2
q^2 = -0.675 GeV^2/c^2
(dσ/d(t-t_min)) photo prod.
σ_U + εσ_L
σ_I
σ_T
15
10
5
0
3
2
-2
-.04
-.08
-.12
t - t_min [GeV^2/c^2]

Fig. 7

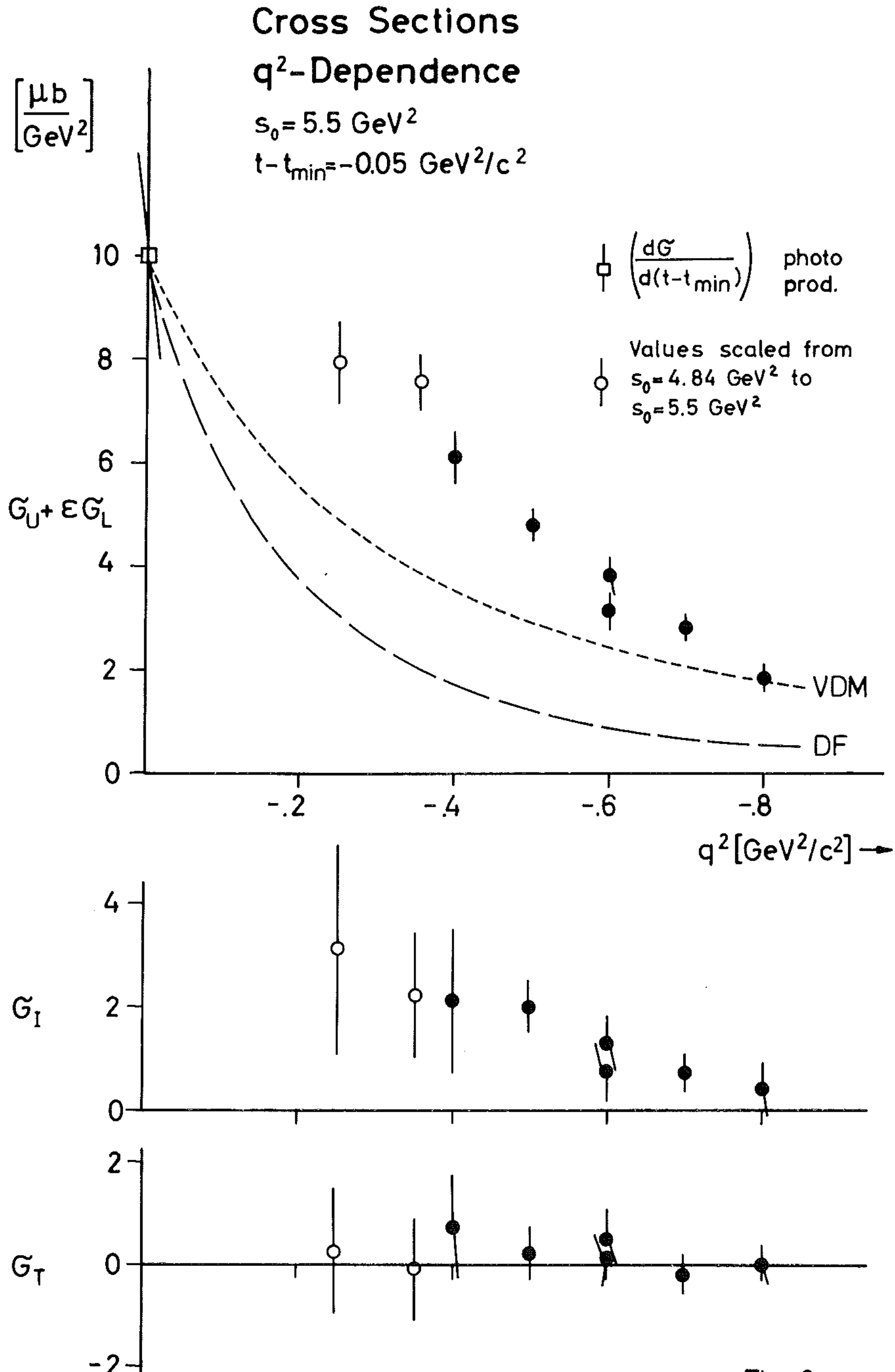
Cross Sections
q²-Dependence
s₀= 5.5 GeV²
t-t_min=-0.05 GeV²/c²
[μb/GeV²]
dσ/d(t-t_min) photo prod.
Values scaled from s₀=4.84 GeV² to s₀=5.5 GeV²
σ_U+ εσ_L
VDM
DF
q²[GeV²/c²]
σ_I
σ_T
10
8
6
4
2
0
-.2
-.4
-.6
-.8
-2

Fig. 8